Supplementary information for

# Detection and identification of Criegee intermediates from the ozonolysis of biogenic and anthropogenic VOCs: comparison between experimental measurements and theoretical calculations

Chiara Giorio[1a]*, Steven J. Campbell[1], Maurizio Bruschi[2], Alexander T. Archibald[1], Markus Kalberer[1]*

[1] Department of Chemistry, University of Cambridge, Lensfield Road, Cambridge, CB2 1EW, United Kingdom
[2] Dipartimento di Scienze dell'Ambiente e del Territorio e di Scienze della Terra, Università degli Studi di Milano Bicocca, Piazza della Scienza 1, Milano, 20126, Italy
[a] now at: Aix-Marseille Université, CNRS, LCE UMR 7376, 13331 Marseille, France

*correspondence to: chiara.giorio@atm.ch.cam.ac.uk; markus.kalberer@atm.ch.cam.ac.uk

## Contents

13 pages

13 figures

2 tables

# S1. Experimental part

## S1.1 Schematic of the flow tube and ozonolysis reaction time

Ozone has been introduced into the flow tube reactor via an 8 mm diameter glass tube of variable length (Figure S1) that allows to vary the reaction time. The outlet of the flow tube is then mixed into a T connection with DMPO in $N_2$ carrier gas. In the configuration used in this study, a residence time in the flow tube of 45 seconds represents the upper limit of the reaction time under the assumption that ozone is immediately mixed with the olefinic precursor at the point in which ozone is injected. However, in our experimental conditions the flow rates of the olefinic precursor (injected at the beginning of the large flow tube) and of ozone (injected through a much narrower tube close to the end of the flow tube) are equal and therefore ozone velocity is about 50 times higher than that of the VOCs. This means that the mixing is turbulent and a better approximation of the actual reaction time is represented by the lower limit that considers that the reaction is happening only at the centre of the flow tube (hatched rectangle in Figure S1).

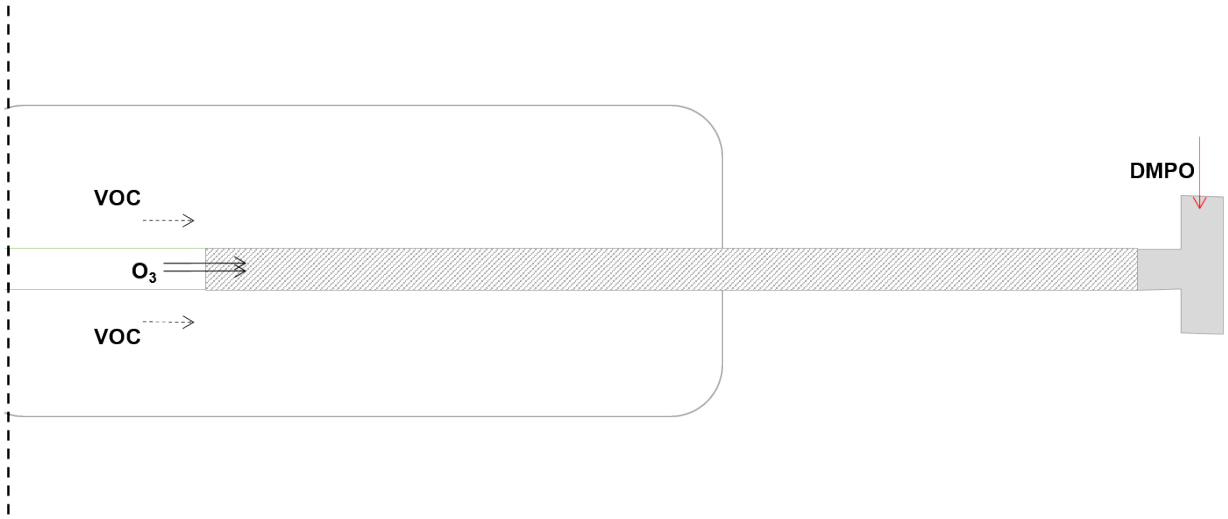


**Figure S 1. Schematic of the final section of the flow tube showing the point in which $O_3$ is mixed with the olefinic VOC and the ozonolysis reaction occurs up to the mixing point with DMPO. The hatched rectangle shows the area considered for calculation of the residence time in the flow tube.**

## S1.2 Measurement of the ozone output from the UV lamp in our experimental set-up

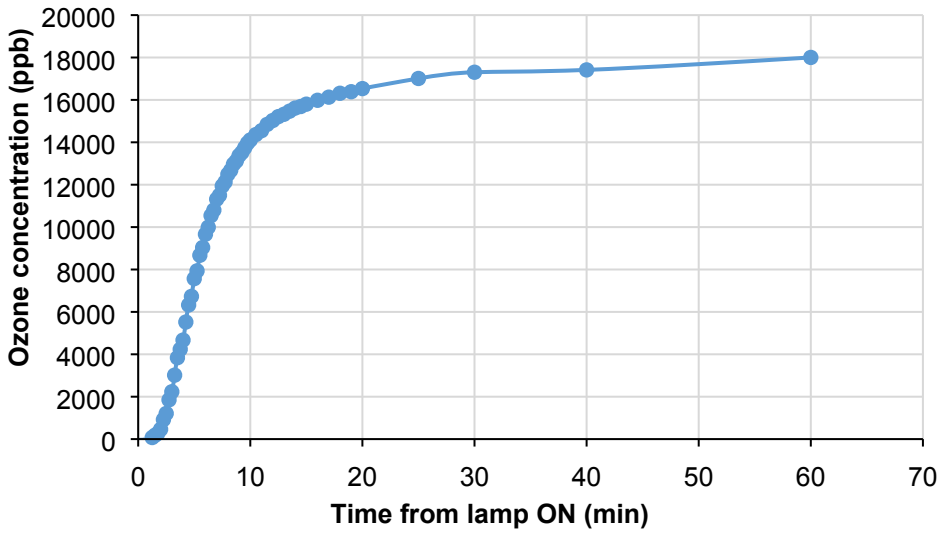


**Figure S 2. Concentration of ozone produced by the UV lamp in our experimental conditions showing the warming up period of the lamp of about 20-30 minutes.**

## S2. Results of AtChem/MCM modelling

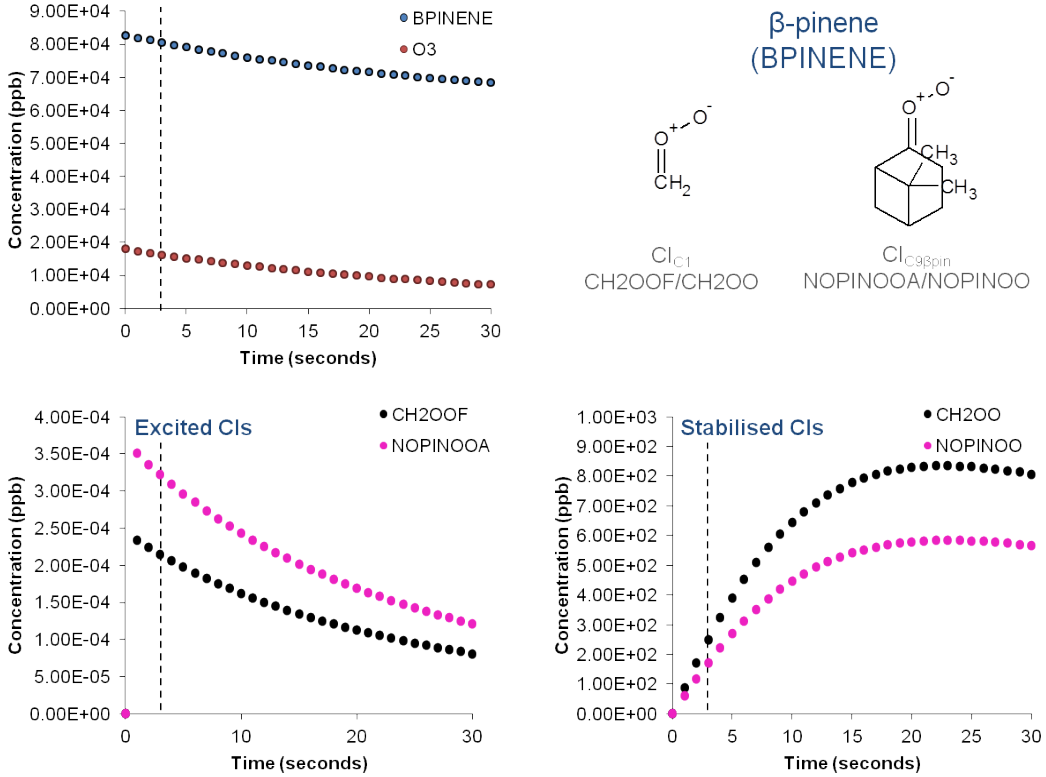


**Figure S 3. Time evolution of precursors, excited CIs and stabilised CIs in the ozonolysis of β-pinene determined by the MCM model simulating our experimental conditions. Dashed vertical bars indicate reaction time in our steady-state flow tube experiments.**

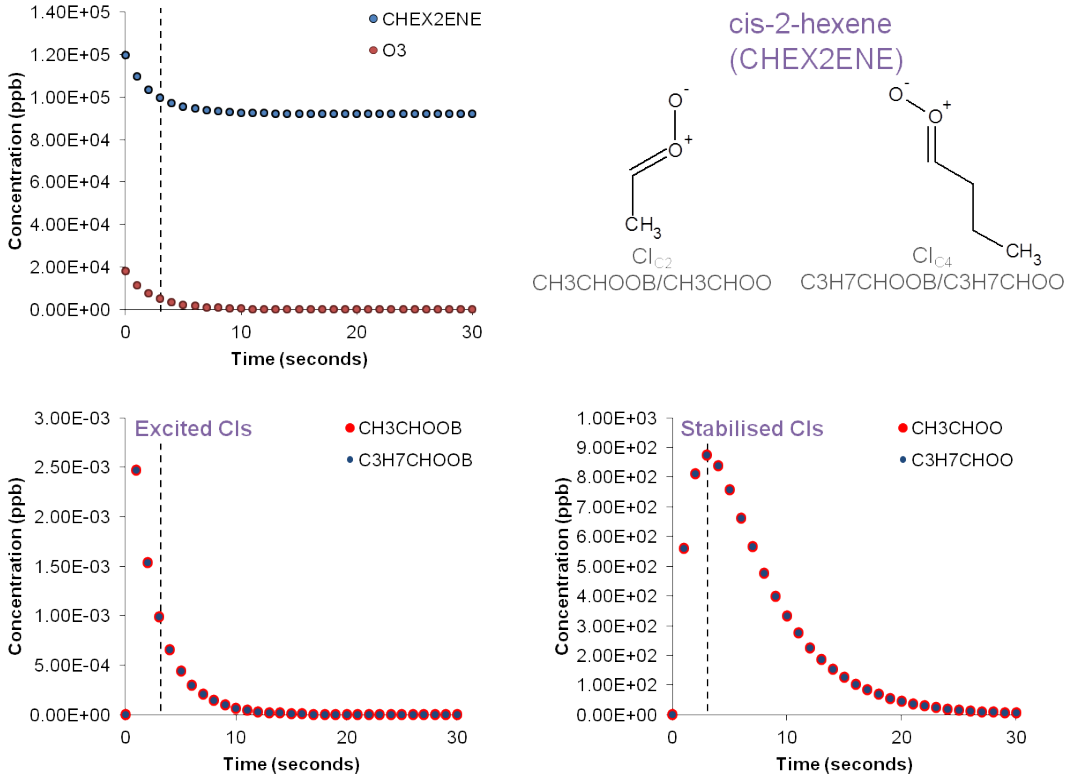


**Figure S 4. Time evolution of precursors, excited CIs and stabilised CIs in the ozonolysis of cis-2-hexene determined by the MCM model simulating our experimental conditions. Dashed vertical bars indicate reaction time in our steady-state flow tube experiments.**

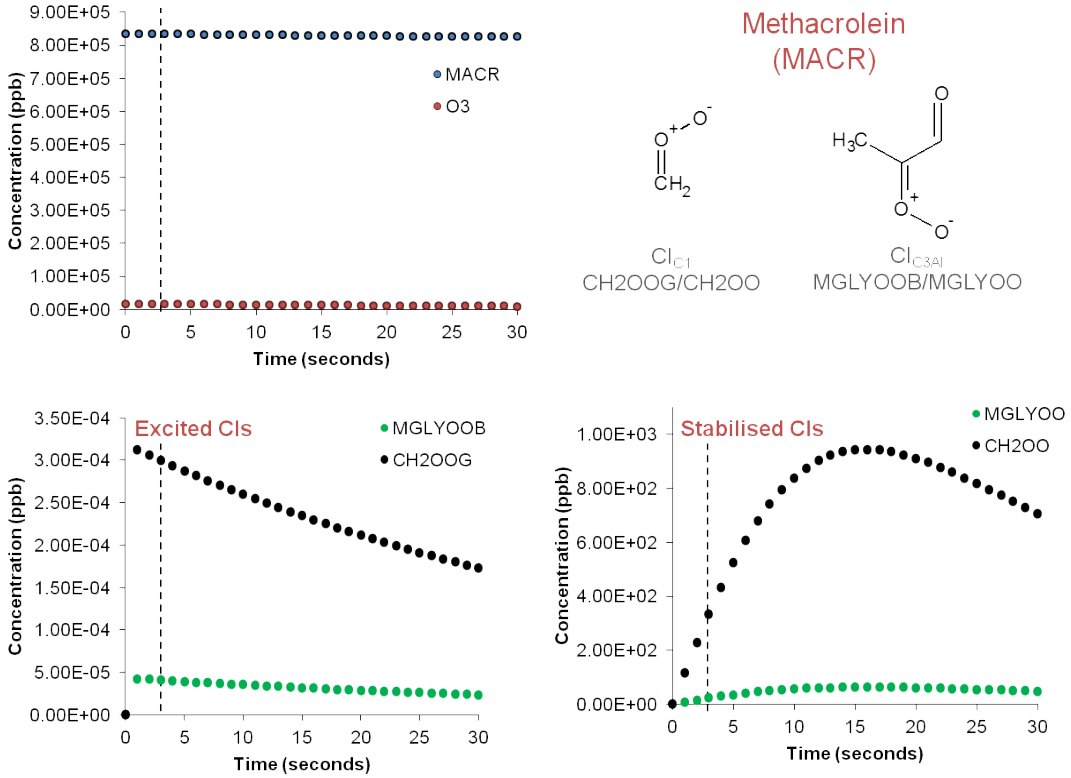


**Figure S 5. Time evolution of precursors, excited CIs and stabilised CIs in the ozonolysis of methacrolein determined by the MCM model simulating our experimental conditions. Dashed vertical bars indicate reaction time in our steady-state flow tube experiments.**

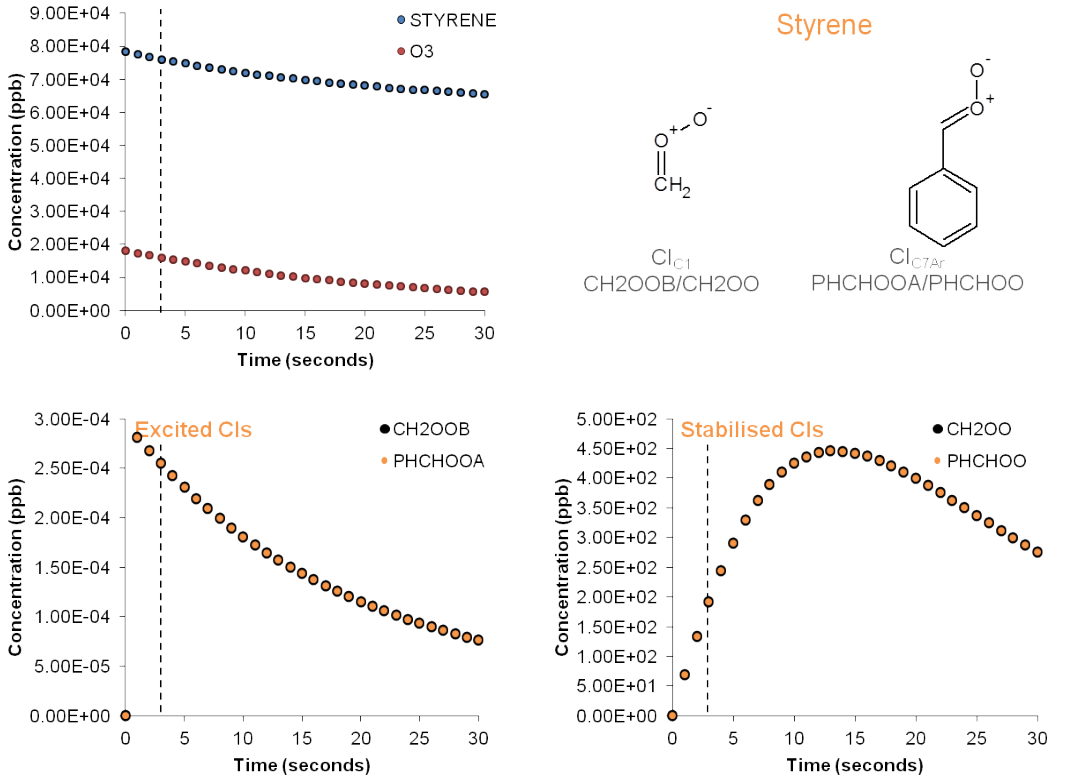


**Figure S 6. Time evolution of precursors, excited CIs and stabilised CIs in the ozonolysis of styrene determined by the MCM model simulating our experimental conditions. Dashed vertical bars indicate reaction time in our steady-state flow tube experiments.**

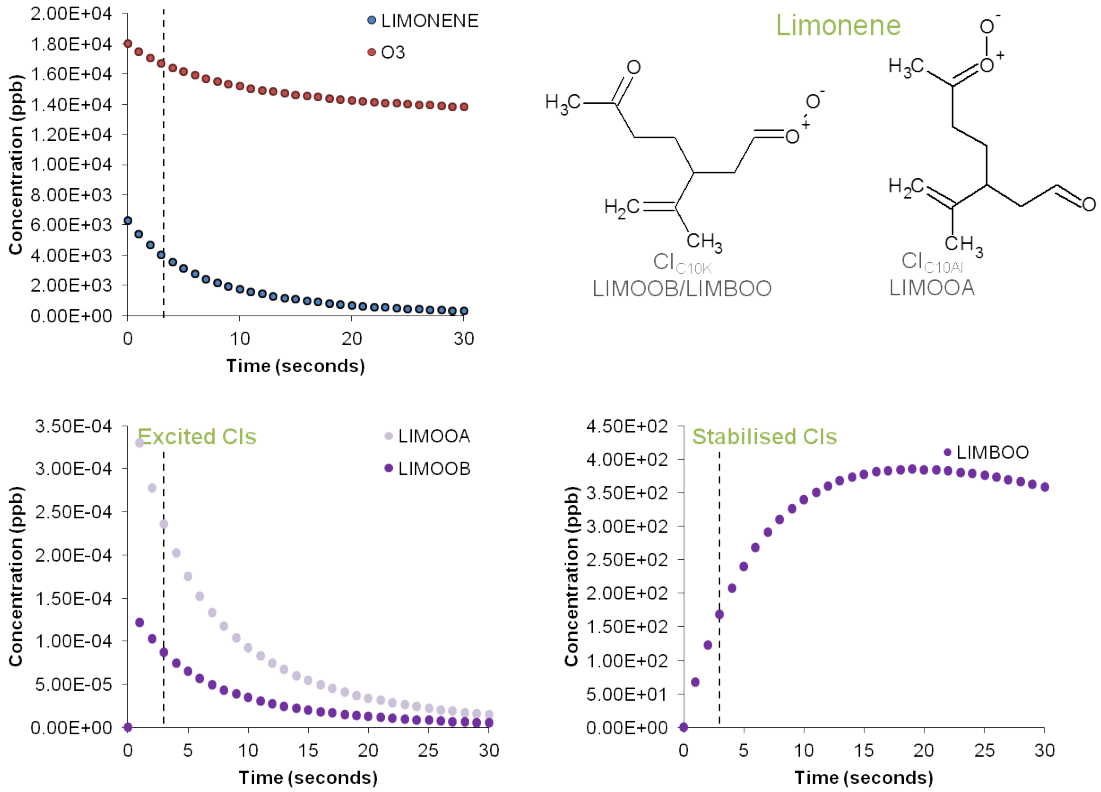


**Figure S 7. Time evolution of precursors, excited CIs and stabilised CIs in the ozonolysis of limonene determined by the MCM model simulating our experimental conditions. Dashed vertical bars indicate reaction time in our steady-state flow tube experiments.**

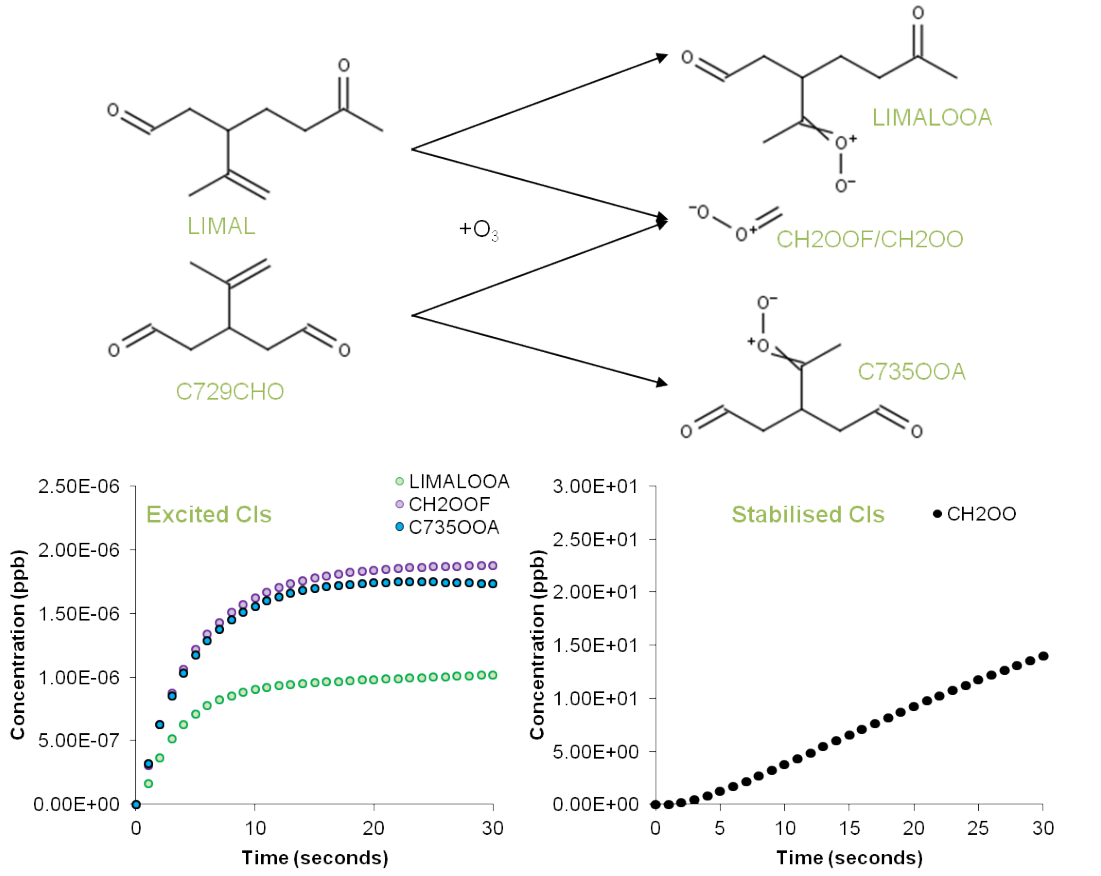


**Figure S 8. Reaction scheme and time evolution of second generation excited CIs and stabilised CIs in the ozonolysis of limonene determined by the MCM model simulating our experimental conditions.**

# S3. DFT calculations

**Table S 1. DFT energies (in Hartree) and thermochemical corrections to absolute enthalpies (H, in kcal/mol) for all of the species investigated in this work calculated using the BP86 and B3LYP functionals. The labels vdw-$CI_X$-DMPO, TS-$CI_X$ –DMPO and $CI_X$-DMPO (X= C1, C2, C4, C3Al, C9βpin) refer to van der Waals pre-reactive complexes, transition states, and the reaction products, respectively. The strings (syn) and (anti) in the labels indicate the initial conformation of the CIs, whereas the strings (RR) and (RS) indicate the absolute configuration of the two stereogenic centres generated in the products by the ring closure of CIs with DMPO. Finally, the string 5R attached to the labels refers to the 5-membered ring adducts.**

| | BP86 | | B3LYP | |
|---|---|---|---|---|
| | **Energy** | **H** | **Energy** | **H** |
| **$CI_{C1}$** | -189.68197749940 | 21.36 | -189.56608692357 | 21.94 |
| **DMPO + $CI_{C1}$** | -555.01039949024 | 126.93 | -554.64398177637 | 130.24 |
| **vdw-$CI_{C1}$-DMPO** | -555.01933673780 | 128.41 | -554.65646613800 | 131.87 |
| **TS-$CI_{C1}$-DMPO** | -555.01468412516 | 128.12 | -554.65561118717 | 131.76 |
| **$CI_{C1}$-DMPO** | -555.07308831951 | 130.12 | -554.71506920591 | 133.82 |
| **$CI_{C1}$-DMPO-5R** | -555.04703275616 | 129.61 | -554.683936602 | 133.60 |
| **$CI_{C2}$(syn)** | -229.02511305612 | 38.65 | -228.880735450 | 39.66 |
| **DMPO + $CI_{C2}$(syn)** | -594.35353504696 | 144.21 | -593.958630303 | 147.96 |
| **VDW-$CI_{C2}$(syn)-DMPO** | -594.36111404340 | 146.14 | -593.969721533 | 149.97 |
| **TS-$CI_{C2}$(syn)-DMPO** | -594.34814898187 | 145.82 | -593.958868203 | 149.76 |
| **$CI_{C2}$(SR)-DMPO** | -594.40278544186 | 147.69 | -594.016522730 | 151.81 |
| **$CI_{C2}$(anti)** | -229.02246054661 | 39.22 | -228.878675730 | 40.20 |
| **DMPO + $CI_{C2}$(anti)** | -594.35088253745 | 144.79 | -593.956570583 | 148.50 |
| **VDW-$CI_{C2}$(anti)-DMPO** | -594.35849683240 | 146.23 | -593.968284404 | 150.01 |
| **TS-$CI_{C2}$(anti)-DMPO** | -594.35244515432 | 145.81 | -593.964380148 | 149.77 |
| **$CI_{C2}$(RR)-DMPO** | -594.40817229023 | 147.72 | -594.022152751 | 151.83 |
| **$CI_{C2}$(RR)-DMPO-5R** | -594.38261459064 | 146.81 | -593.988990663 | 151.40 |
| **$CI_{C4}$(syn)** | -307.67906715252 | 75.68 | -307.478302874 | 77.59 |
| **DMPO + $CI_{C4}$(syn)** | -673.00748914336 | 181.24 | -672.556197727 | 185.89 |
| **vdw-$CI_{C4}$(syn)-DMPO** | -673.01205253420 | 182.01 | -672.565426987 | 186.72 |
| **TS-$CI_{C4}$(syn)-DMPO** | -673.00099221696 | 181.54 | -672.555009986 | 187.01 |
| **$CI_{C4}$(SR)-DMPO** | -673.05474023645 | 183.82 | -672.611734008 | 188.83 |
| **$CI_{C4}$(anti)** | -307.67528323976 | 75.54 | -307.474896944 | 77.42 |
| **DMPO + $CI_{C4}$(anti)** | -673.00370523060 | 181.10 | -672.552791797 | 185.72 |

| | | | | |
|---|---|---|---|---|
| **vdw-$CI_{C4}$(anti)-DMPO** | -673.00940307680 | 182.40 | -672.562848272 | 187.08 |
| **TS-$CI_{C4}$(anti)-DMPO** | -673.00333738532 | 181.93 | -672.558740053 | 186.79 |
| **$CI_{C4}$(RR)-DMPO** | -673.05966652739 | 183.90 | -672.617029816 | 188.90 |
| **$CI_{C4}$(RR)-DMPO-5R** | -673.03285895590 | 182.97 | -672.582643115 | 188.35 |
| | | | | \ |
| **$CI_{C3Al}$(syn)** | -342.40508943203 | 46.07 | -342.19458759906 | 47.27 |
| **DMPO + $CI_{C3Al}$(syn)** | -707.73351142287 | 151.64 | -707.27248245186 | 155.57 |
| **vdw-$CI_{C3Al}$(syn)-DMPO** | -707.73828050660 | 152.99 | -707.28049788530 | 156.99 |
| **TS-$CI_{C3Al}$(syn)-DMPO** | -707.71498330624 | 152.52 | -707.26195558854 | 156.42 |
| **$CI_{C3Al}$(RR)-DMPO** | -707.76437787700 | 153.62 | -707.31560624317 | 158.07 |
| **$CI_{C3Al}$(anti)** | -342.39404549779 | 45.97 | -342.18512800976 | 47.17 |
| **DMPO + $CI_{C3Al}$(anti)** | -707.72246748863 | 151.54 | -707.26302286256 | 155.48 |
| **vdw-$CI_{C3Al}$(anti)-DMPO** | -707.73457311570 | 152.89 | -707.27777834710 | 156.90 |
| **TS-$CI_{C3Al}$(anti)-DMPO** | -707.72207888862 | 152.38 | -707.26926796583 | 156.96 |
| **$CI_{C3Al}$(SR)-DMPO** | -707.77068640555 | 153.90 | -707.32087364105 | 158.21 |
| **$CI_{C3Al}$(RR)-DMPO-5R** | -707.74239011534 | 153.50 | -707.28440450926 | 158.13 |
| **$CI_{C9\beta pin}$(anti)** | -501.87605827546 | 137.34 | -501.53402337817 | 140.92 |
| **DMPO + $CI_{C9\beta pin}$(anti)** | -867.20448026630 | 242.91 | -866.61191823097 | 249.23 |
| **vdw-$CI_{C9\beta pin}$(anti)-DMPO** | -867.20966062030 | 244.25 | -866.59489872625 | 250.29 |
| **TS-$CI_{C9\beta pin}$(anti)-DMPO** | -867.18321142654 | 243.80 | -866.59478879625 | 250.29 |
| **$CI_{C9\beta pin}$(RR)-DMPO** | -867.23883564418 | 245.34 | -866.65341721554 | 252.02 |
| **$CI_{C9\beta pin}$(syn)** | -501.87230381852 | 137.48 | -501.53027166177 | 140.49 |
| **DMPO + $CI_{C9\beta pin}$(syn)** | -867.20072580936 | 243.05 | -866.60816651457 | 248.79 |
| **vdw-$CI_{C9\beta pin}$(syn)-DMPO** | -867.20702411540 | 244.49 | -866.61754549743 | 250.53 |
| **TS-$CI_{C9\beta pin}$(syn)-DMPO** | -867.18589340982 | 243.77 | -866.59619578036 | 250.28 |
| **$CI_{C9\beta pin}$(SR)-DMPO** | -867.23983887076 | 245.34 | -866.65410809670 | 252.03 |

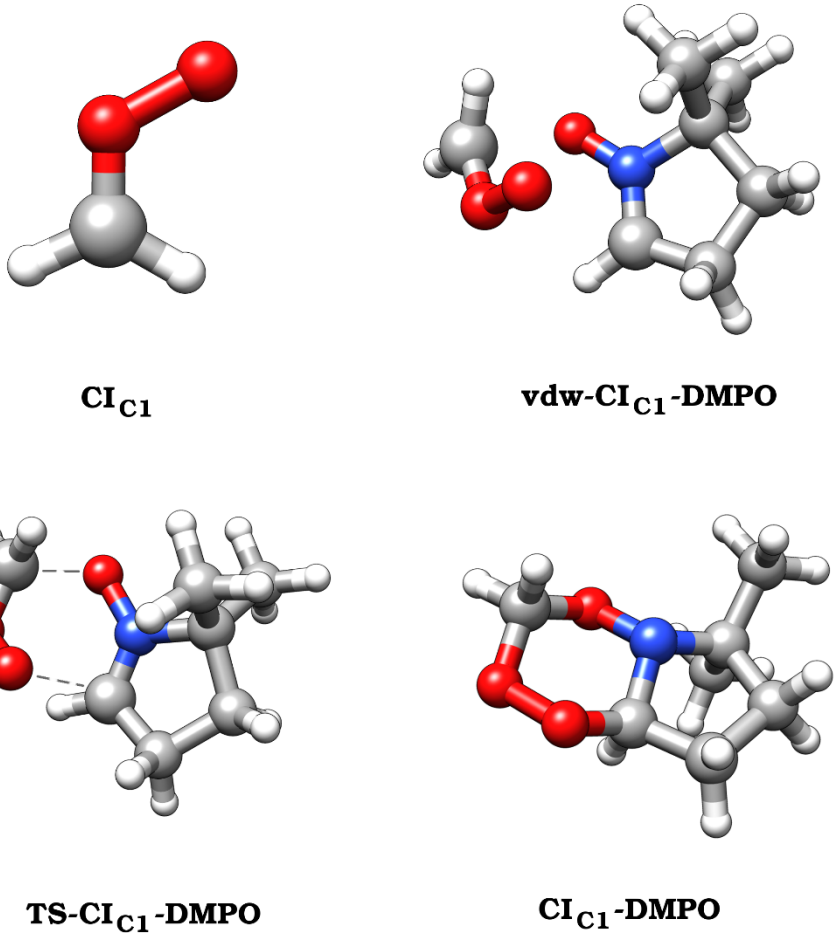


**Figure S 9. DFT-B3LYP optimized structures of $CI_{C1}$, and the relevant species formed along the pathway of the reaction of $CI_{C1}$ and DMPO. For the labels, see the caption of Table S1**

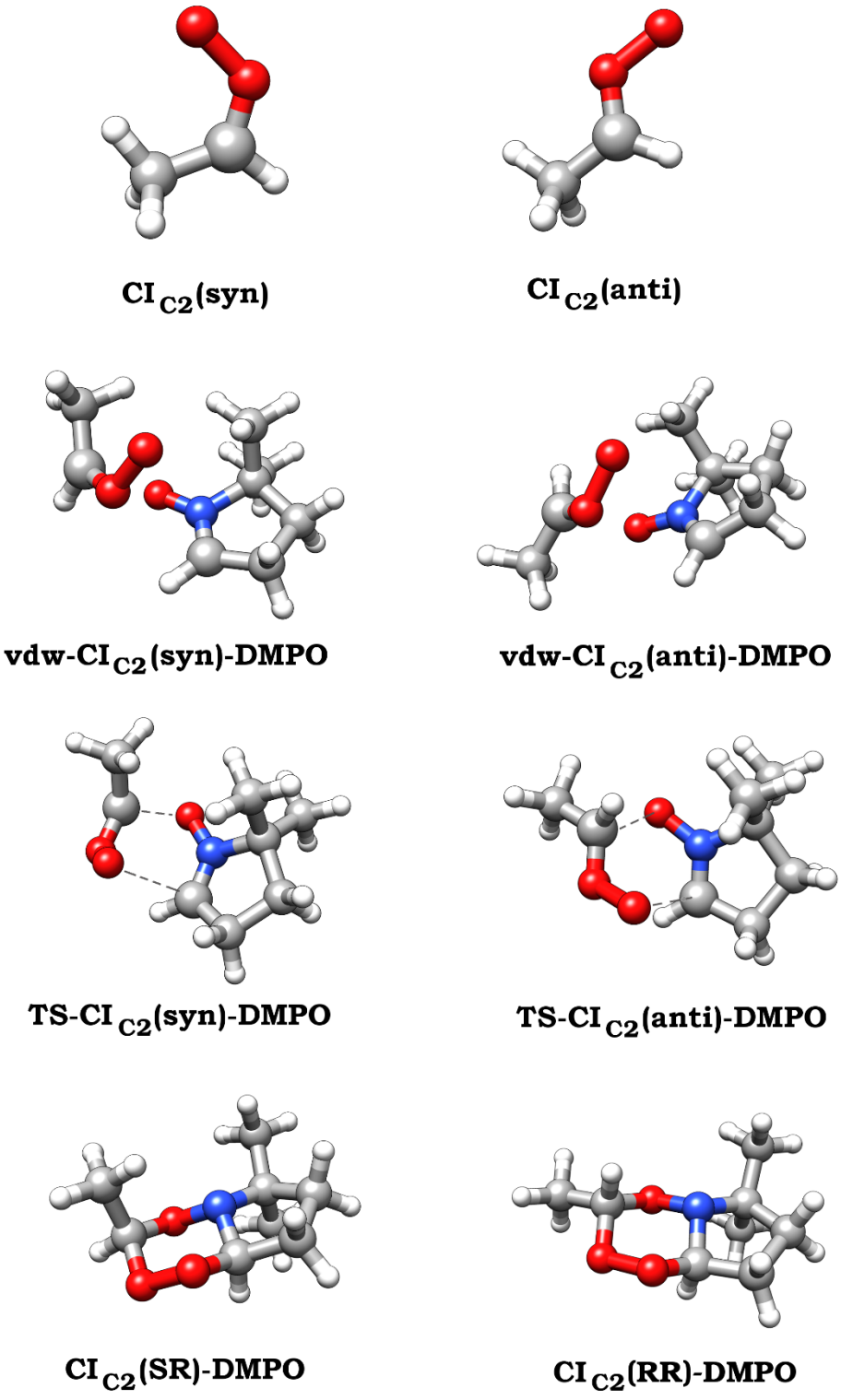


**Figure S 10. DFT-B3LYP optimized structures of $CI_{C2}$, and the relevant species formed along the pathway of the reaction of $CI_{C2}$ and DMPO. For the labels, see the caption of Table S1**

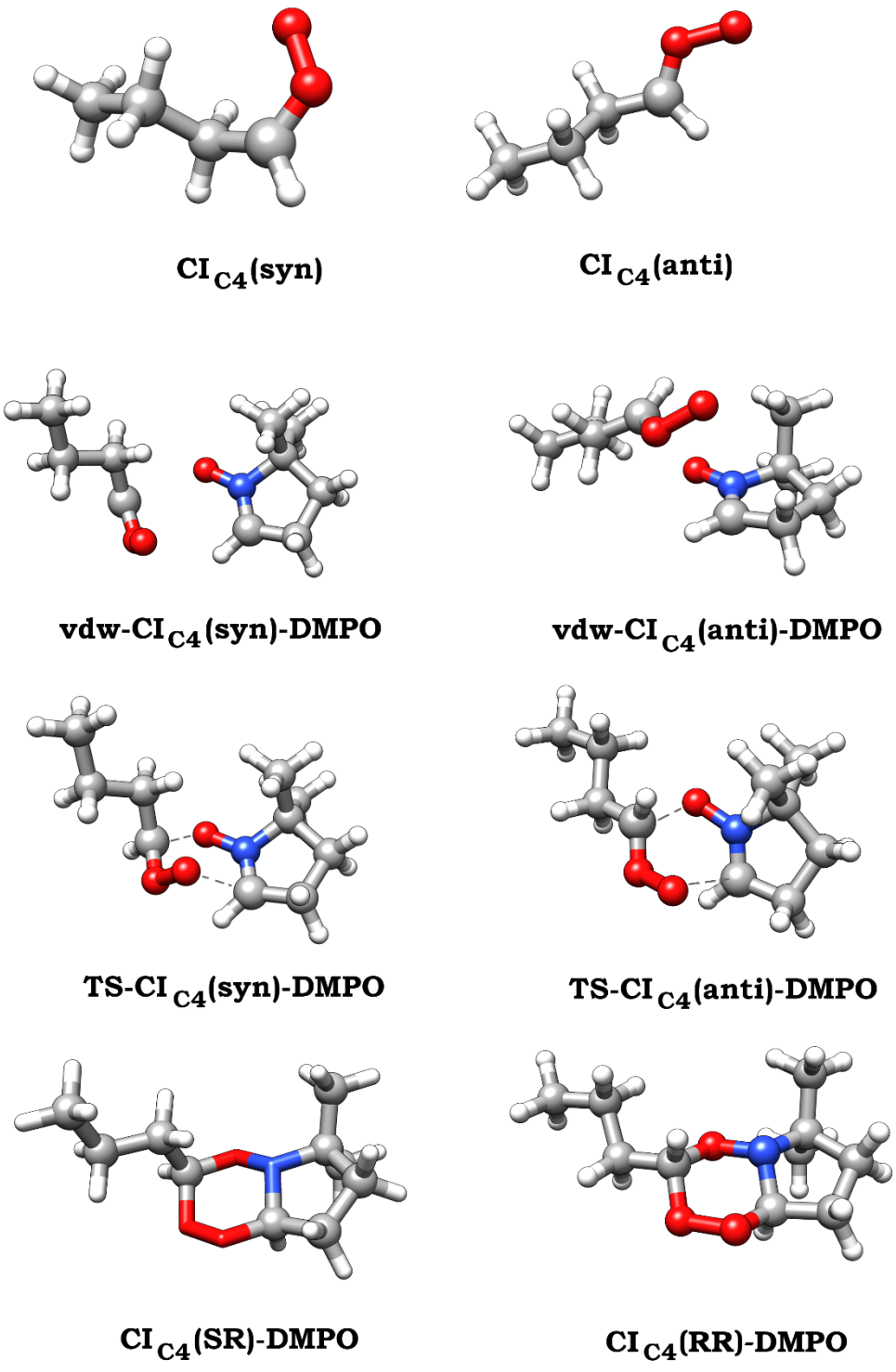


**Figure S 11. DFT-B3LYP optimized structures of $CI_{C4}$, and the relevant species formed along the pathway of the reaction of $CI_{C4}$ and DMPO. For the labels, see the caption of Table S1**

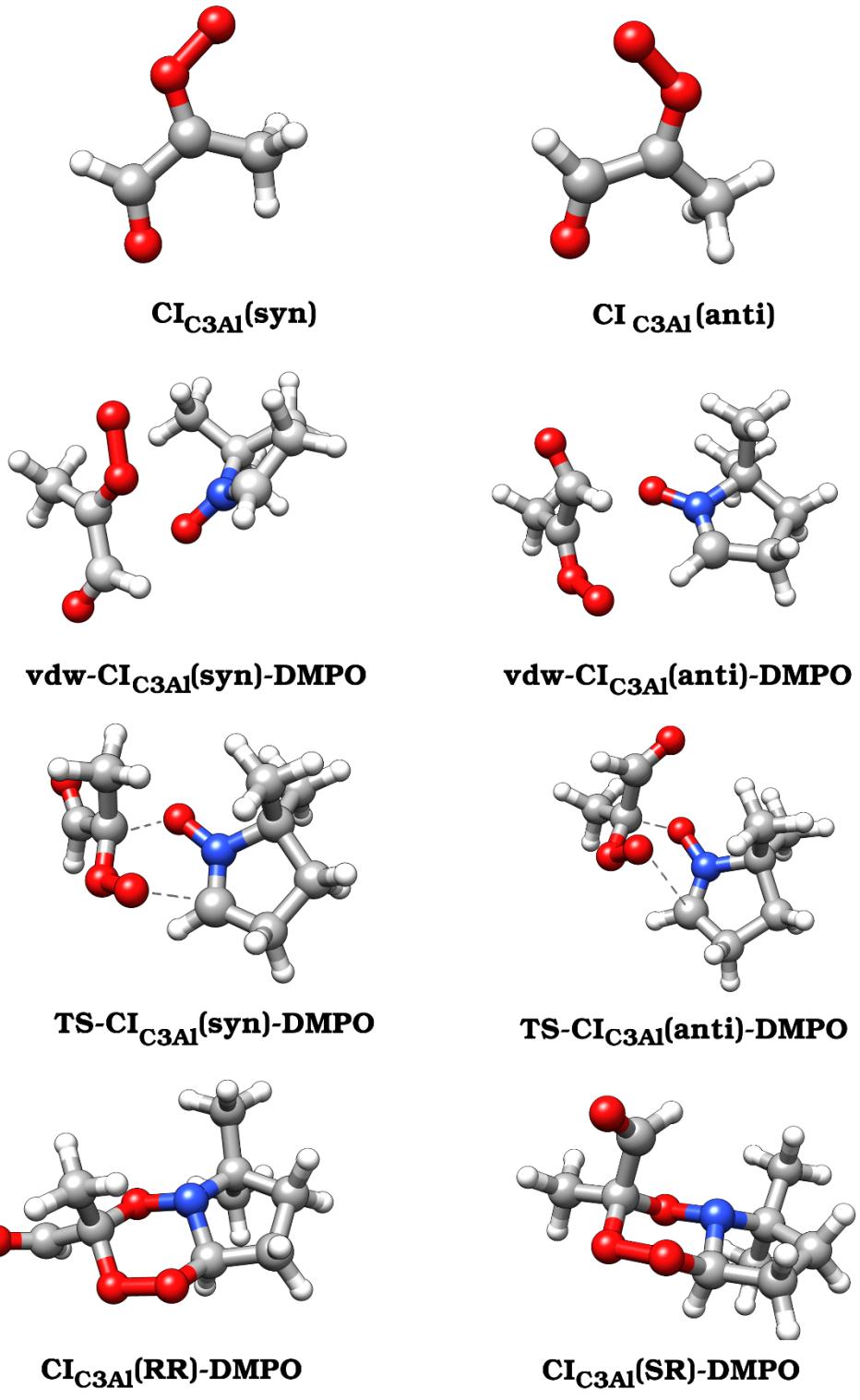


**Figure S 12. DFT-B3LYP optimized structures of $CI_{C3Al}$, and the relevant species formed along the pathway of the reaction of $CI_{C4}$ and DMPO. For the labels, see the caption of Table S1**

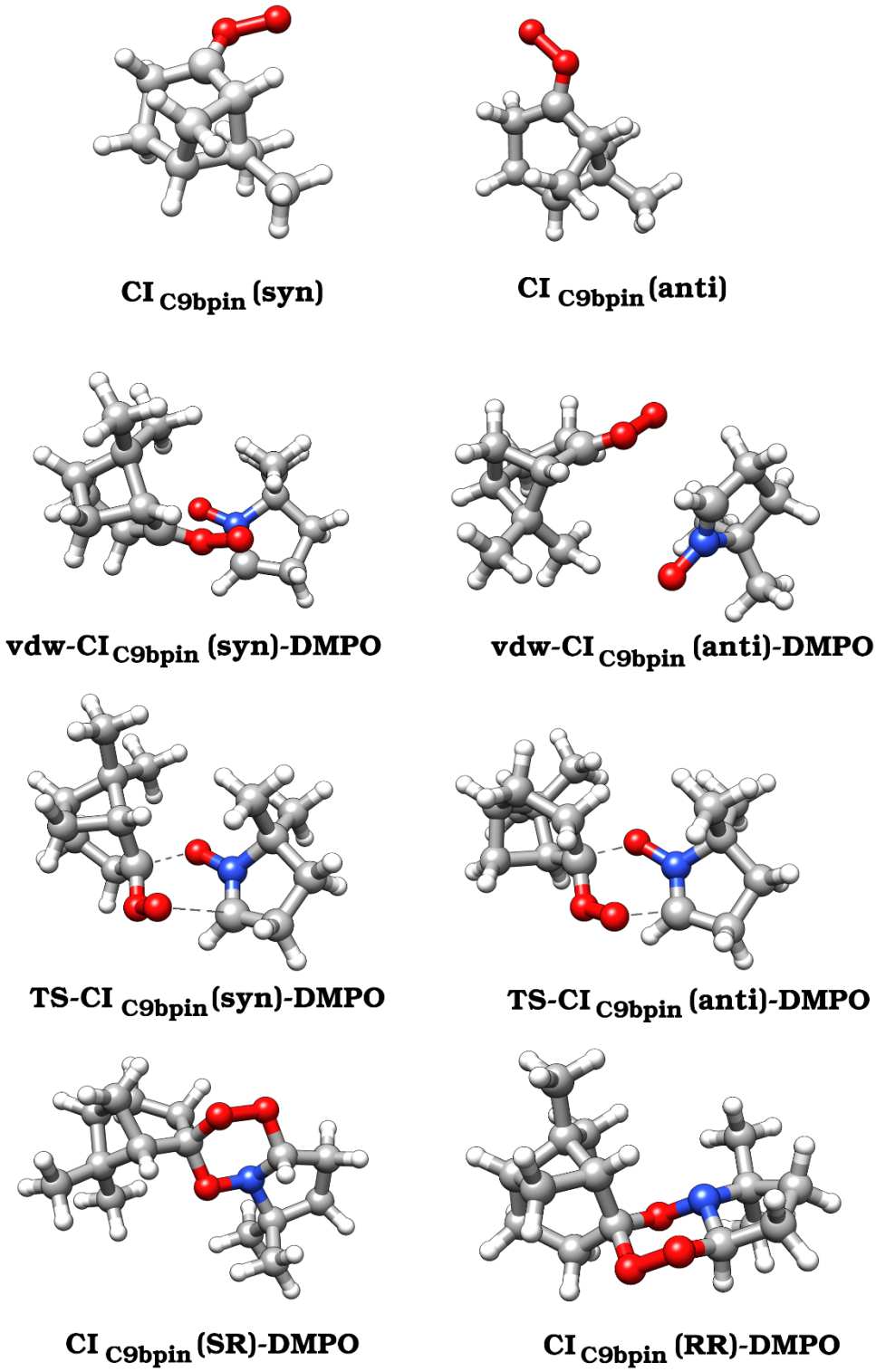


**Figure S 13. DFT-B3LYP optimized structures of $CI_{9\beta pin}$, and the relevant species formed along the pathway of the reaction of $CI_{C9\beta pin}$ and DMPO. For the labels, see the caption of Table S1**

## S4. Theoretical calculations of proton transfer reaction rate coefficients

Proton transfer reaction rates for DMPO and all CIs-DMPO adducts have been calculated using the Langevin model, describing a long range interaction between a point charge and a polarisable molecule,[1] the average-dipole-orientation theory (ADO) which considers also the permanent dipole moment of the neutral organic species,[1] and the refined ADO theory parametrised by Su and Chesnavich[2] to account for the kinetic energy dependence of the rate constant across a wide range of temperatures. Average static polarizability and the dipole moment of the DMPO and CIs-DMPO adducts were calculated using the B3LYP/def-TZVP level of theory as described in the main text (section 2.4). Details on the calculations of proton transfer rate coefficients using the three different theories can be found elsewhere.[3,4] Rate constants of DMPO and CIs-DMPO adducts for T=300K and a drift tube temperature of 363.15K, as used in this study, are reported in Table S2. An average of $k_{cap}$ at 363.15K for the RR and SR orientations of each molecule and an average of the $k_{cap}$ for $CI_{C10Al}$ and $CI_{C10K}$ were used for quantification of all CIs-DMPO adducts.

**Table S2. Polarizability, dipole moment, Langevin collision rate constant ($k_L$), ADO collision rate constant ($k_{ADO}$) and ion-polar molecule capture collisions rate constant ($k_{cap}$) at 300K and 363.15K (operating drift tube temperature in our experiments).**

| Compound | α (Å$^3$) | $\mu_D$ (D) | T (K) | $k_L$ (x10$^{-9}$ cm$^3$ s$^{-1}$) | $k_{ADO}$ (x10$^{-9}$ cm$^3$ s$^{-1}$) | $k_{cap}$ (x10$^{-9}$ cm$^3$ s$^{-1}$) |
|---|---|---|---|---|---|---|
| **DMPO** | 12.06 | 4.07 | 300 | 2.02 | 4.34 | 2.77 |
| | | | 363.15 | 2.02 | 4.13 | 2.75 |
| **$CI_{C3Al}$ (RR)-DMPO** | 18.42 | 4.8 | 300 | 2.41 | 5.04 | 3.37 |
| | | | 363.15 | 2.41 | 4.80 | 3.35 |
| **$CI_{C3Al}$ (SR)-DMPO** | 18.49 | 4.84 | 300 | 2.42 | 5.07 | 3.37 |
| | | | 363.15 | 2.42 | 4.83 | 3.35 |
| **$C_{9bpin}$ (RR)-DMPO** | 27.55 | 2.144 | 300 | 2.92 | 3.79 | 3.25 |
| | | | 363.15 | 2.92 | 3.71 | 3.22 |
| **$C_{9bpin}$ (SR)-DMPO** | 27.38 | 2.073 | 300 | 2.91 | 3.74 | 3.21 |
| | | | 363.15 | 2.91 | 3.67 | 3.19 |
| **$CI_{C1}$ (R)-DMPO** | 14.66 | 2.558 | 300 | 2.18 | 3.44 | 3.01 |
| | | | 363.15 | 2.18 | 3.33 | 2.95 |
| **$CI_{C4}$ (RR)-DMPO** | 20.27 | 2.378 | 300 | 2.53 | 3.61 | 3.07 |
| | | | 363.15 | 2.53 | 3.51 | 3.03 |
| **$CI_{C4}$ (SR)-DMPO** | 19.96 | 2.283 | 300 | 2.51 | 3.53 | 3.01 |
| | | | 363.15 | 2.51 | 3.44 | 2.97 |
| **$CI_{C2}$ (RR)-DMPO** | 16.61 | 2.294 | 300 | 2.31 | 3.37 | 2.89 |
| | | | 363.15 | 2.31 | 3.28 | 2.85 |
| **$CI_{C2}$ (SR)-DMPO** | 16.35 | 2.400 | 300 | 2.29 | 3.43 | 2.94 |
| | | | 363.15 | 2.29 | 3.33 | 2.90 |
| **$CI_{C7Ar}$ (RR)-DMPO** | 24.67 | 2.339 | 300 | 2.77 | 3.78 | 3.22 |
| | | | 363.15 | 2.77 | 3.69 | 3.19 |
| **$CI_{C9lim}$ (RR)-DMPO** | 28.40 | 2.068 | 300 | 2.96 | 3.78 | 3.26 |
| | | | 363.15 | 2.96 | 3.71 | 3.24 |
| **$CI_{C10Al}$ (RR)-DMPO** | 34.45 | 4.921 | 300 | 3.28 | 5.82 | 4.78 |
| | | | 363.15 | 3.28 | 5.59 | 4.74 |
| **$CI_{C10K}$ (RR)-DMPO** | 30.95 | 4.847 | 300 | 3.08 | 5.59 | 4.48 |
| | | | 363.15 | 3.08 | 5.36 | 4.45 |

## References


1 R. S. Blake, P. S. Monks and A. M. Ellis, *Chem. Rev.*, 2009, **109**, 861–896.

2 T. Su and W. J. Chesnavich, *J. Chem. Phys.*, 1982, **76**, 5183–5185.

3 L. Cappellin, M. Probst, J. Limtrakul, F. Biasioli, E. Schuhfried, C. Soukoulis, T. D. Märk and F. Gasperi, *Int. J. Mass Spectrom.*, 2010, **295**, 43–48.

4 T. Su, *J. Chem. Phys.*, 1994, **100**, 4703–4703.